Letter

Large and tunable spin-orbit effect of 6*p* orbitals through structural cavities in crystals

Mauro Fava [1,*] William Lafargue-Dit-Hauret [1,2] Aldo H. Romero [3] and Eric Bousquet [1]

[1]*Physique Théorique des Matériaux, QMAT, CESAM, Université de Liège, B-4000 Sart-Tilman, Belgium*

[2]*Universite de Pau et des Pays de l'Adour, E2S UPPA, CNRS, IPREM, 64000 Pau, France*

[3]*Department of Physics and Astronomy, West Virginia University, Morgantown, West Virginia 26505-6315, USA*

(Received 9 May 2023; accepted 24 October 2023; published 14 November 2023; corrected 15 February 2024)

We explore from first-principles calculations the ferroelectric material $Pb_5Ge_3O_{11}$ as a model for controlling the spin-orbit interaction (SOC) in crystalline solids. The SOC has a surprisingly strong effect on the structural energy landscape by deepening the ferroelectric double well. We observe that this effect comes from a specific Pb Wyckoff site that lies on the verge of a natural cavity channel of the crystal. We also find that a unique cavity state is formed by the empty 6*p* states of another Pb site at the edge of the cavity channel. This cavity state exhibits a sizable spin splitting with a mixed Rashba-Weyl character and a topologically protected crossing of the related bands. We also show that the ferroelectric properties and the significant SOC effects are exceptionally robust in the presence of n-type doping at levels of up to several electrons per unit cell. We trace the provenance of these original effects to the unique combination of the structural cavity channel and the chemistry of the Pb atoms with 6*p* orbitals localizing inside the channel.

DOI: 10.1103/PhysRevB.108.L201112

Relativistic atomic spin-orbit coupling (ASOC) was first introduced in the early 1930s during the development of quantum mechanics. It refers to the interaction between the electronic spin **S** and its angular momentum **L**. Even though ASOC is weak compared with Coulomb or kinetic interactions (one to two orders of magnitude) and even weaker in molecules or crystals owing to the quenching of **L** with chemical bonding, it appears to be the fundamental interaction to describe, for example, the atomic magnetic moment directions (magnetic anisotropy), magnetostriction or spin canting, and weak ferromagnetism [1]. Hence spin-orbit coupling (SOC) has been a centerpiece of molecular and condensed matter physics, and a recent revival of interest is now at play with the discovery of new SOC-related phenomena such as spin torques [2,3], skyrmions [4–6], the presence of a topological $\mathbb{Z}_2$ order [7,8], the quantum spin-Hall effect [9–12], the existence of spin states with long lifetimes [13–17], linear [18–22] and cubic [23–25] Rashba (R) and Dresselhaus (D) spin splitting, and so on. These new phenomena are significant for future spintronic applications. The term "spin-orbitronics" is also adopted when the SOC is the driving ingredient [26].

Thus, controlling spin-orbital features is paramount for realizing numerous phenomena with high technological impact. On the other hand, finding a single material that encompasses several useful and significant SOC features and guarantees, as a matter of principle, a reasonable degree of handling over the "internal" parameters is difficult. Furthermore, concerning the Rashba physics, which requires doping to be harnessed in polar insulators, a known problem is the preservation of the mirror symmetry breaking in doping conditions since screening by free charges tends to destabilize the electric polarization [27]. In this Research Letter, we address both issues at once. We use the ferroelectric axial [28,29] compound lead germanate oxide $Pb_5Ge_3O_{11}$ (PGO) [30,31] as a single platform for the manipulation of spin-orbit interaction. We show from density functional theory (DFT) calculations (see Supplemental Material [32] and Refs. [33–40] therein) that SOC has an unexpectedly significant impact on both the structural energy landscape of PGO and its electronic structure with a mixed Rashba-Weyl crossing between the spin bands, which is topologically protected by a $\mathbb{Z}_2$ invariant. More specifically, we show that this significant SOC effect originates from two unique features: (i) a vacuum channel in the crystal structure that localizes and unquenches the empty 6*p* orbitals of some specific lead cations and (ii) the breaking of the mirror site symmetry at other Pb sites. In addition, we show that, unlike common ferroelectric materials, the ferroelectric energy is enhanced by negative carrier doping, which we explain in terms of the short-range nature of the polar instability and localization of the aforementioned 6*p* states. From these results, we discuss the design rules for controlling spin-orbital features in solid materials.

PGO is a band-gap insulator that undergoes a ferroelectric structural phase transition at 450 K [30]. Hence it is a room-temperature uniaxial ferroelectric (FE) and chiral material ($P3$ space group 143) with a measured spontaneous polarization of $\sim 5\ \mu C/cm^2$ along the c axis. The combination of chirality and ferroelectricity makes PGO gyroelectric and electrogyroelectric, and the natural optical activity can be tuned and switched by an applied electric field following a hysteresis process [41,42]. We provide a schematic view of the high-symmetry $P\bar{6}$ phase (space group 174) in Fig. 1. The unit cell of PGO contains 57 atoms, and the paraelectric (PE) and FE phases are described by 15 and 23 asymmetric Wyckoff positions (WPs), respectively. The crystal structure can

*mfava@uliege.be

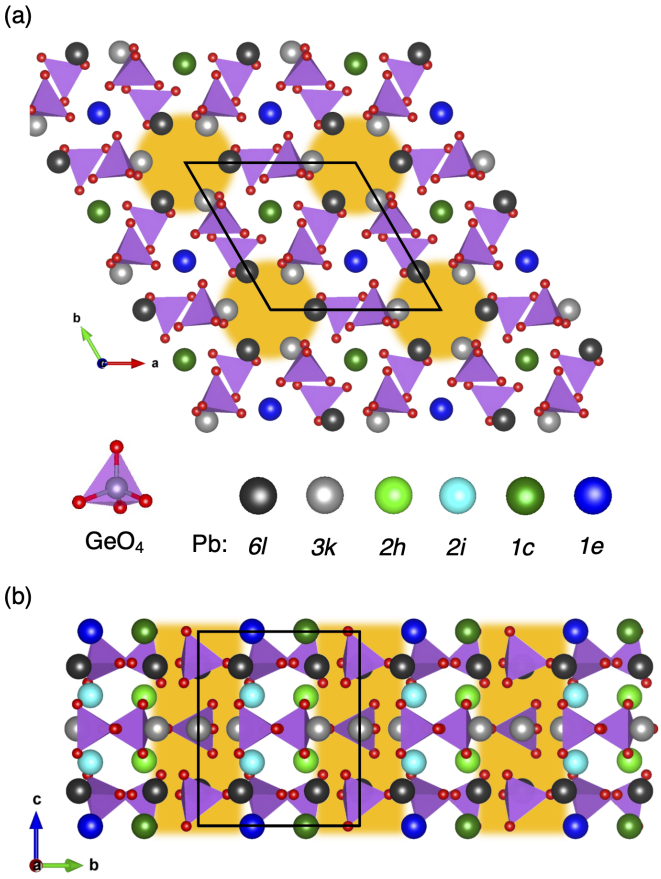

FIG. 1. Top (a) and side (b) views of PGO (PE phase). Oxygen atoms are shown in red, and Ge atoms and germanate units are shown in purple, while the lead ions are distinguished by their Wyckoff positions. Empty channels are evidenced in gold.

be described as follows. The germanium atoms form—along with the surrounding oxygen atoms—either GeO_4 tetrahedra ($z = 0.5$, $6l$ WP) or Ge_2O_7 dimers ($z = 0$, $3k$ WP). The lead atoms bridge the Ge_2O_7 and GeO_4 units. Pb atoms can be separated into two groups. The first group of Pb atoms are located in $6l$ and $3k$ WPs (black and gray atoms in Fig. 1) and form empty hexagonal channels that propagate along the [001] crystallographic direction (highlighted in gold in Fig. 1). The second group consists of Pb atoms found between these channels, that is, the $1e$, $1c$, $2i$, and $2h$ WPs (dark blue, dark green, cyan, and lime atoms in Fig. 1). Owing to the loss of mirror symmetry in the FE phase, the Pb-$6l$ positions split into two pairs of $3d$ WPs (at the top and at the bottom of the unit cell, respectively) in the $P3$ phase.

We start by performing the optimization of the lattice parameters, which are also in good agreement (see Supplemental Material [32]) with their measured values [30,43,44]. Defining $\Delta E = E(P\bar{6}) - E(P3)$ as the energy gain between the paraelectric phase and the ferroelectric phase, we obtain $\Delta E(\text{no SOC}) = 68$ meV in the absence of SOC and $\Delta E(\text{with SOC}) = 89$ meV when the SOC is included in the calculation, i.e., an increase of 31%. This means that the ferroelectric double-well depth of PGO is strongly sensitive to the spin-orbit interaction. Furthermore, the SOC enhancement of ΔE is typically not as prominent in lead-based ferroelectrics such as $PbTiO_3$ [45]. Thus these preliminary results call for a deeper investigation of the electronic properties to understand the significant effect of SOC on the ferroelectric well depth.

In Fig. 2(a), right panel, we report the *spd*-projected density of states (DOS) around the last occupied valence state and the first unoccupied conduction state of the FE $P3$ phase. The top valence band (VB) is dominated by O-$2p$ states followed by contributions from the Pb-$6s$ states and, in a small amount, the Pb-$6p$ states, suggesting sizable covalent hybridization between the oxygen and lead. The contributions from the d orbitals are almost absent because, as expected, both Ge and Pb d orbitals are far lower in energy (approximately -10 eV). The conduction bands (CBs) are dominated by the Pb-$6p$ spectral weight and show a large Pb-$6p$–O-$2p$ hybridization (plus Pb-$6s$–O-$2p$ hybridization in a smaller amount). In the left panel of Fig. 2(a), we report the electronic band structure of the $P3$ phase in the presence and absence of SOC. In the $P3$ ($P\bar{6}$) phase without SOC we obtain a band gap of 2.48 (2.35) eV, which is reduced to 2.25 (2.11) eV if the SOC is included. It is shown in the Supplemental Material that ΔE is negatively correlated with the gap size, experimentally found to be 3 eV [46,47]. While SOC has only a small effect on the valence band maximum, which has mostly oxygen character, its impact on the CB is sizable.

To better analyze and quantify the effect of spin-orbit interaction, we performed an irreducible representation (IR) analysis of the VB maximum (VBM) and CB minimum (CBM) states at the Γ point [32]. A scheme of SOC-induced splitting for the $P3$ phase is highlighted in Fig. 2(b). When the SOC is switched off, the top VB is populated by states belonging to the invariant representation of either the C_{3h} or C_3 point groups, whereas the bottom CB is constituted by p_x and p_y orbitals (E' and E single representations of C_{3h} and C_3, respectively), with a state belonging to the invariant representation (Γ_1) located higher in energy. With reference to the conduction bands in the $P3$ phase we define $\gamma = |E(\bar{\Gamma}_4) - E(D_{1/2})|$, with the split-off energy between the invariant and the p_x and p_y orbitals in the absence of SOC as its upper bound. Clearly, the ferroelectric phase transition does not affect the in-plane p levels, and adding the spin-orbit coupling results in additional splitting, which in the FE case can be defined as $\delta = |E(\bar{\Gamma}_5 \oplus \bar{\Gamma}_6) - E(\bar{\Gamma}_4)|$. From our calculations, we obtain $\delta = 180$ meV, whereas γ is reduced from 270 meV (no SOC) to 106 meV (with SOC). Such a large SOC effect on the electronic band structure is approximately of the same order of magnitude as that of bulk Au [48], but it is unexpected for ferroelectric insulators with Pb^{2+} cations such as $PbTiO_3$ [45]. Unlike the case of halide perovskites such as $CsPbBr_3$ [49], the singlet-triplet SOC-induced inversion does not occur.

In addition, the orbital angular momentum $\mathbf{L}$ over the Γ-CBM states is unquenched [32], which means that the SOC is a first-order correction $\sim \langle \mathbf{L} \rangle \cdot \mathbf{S}$ of the electronic energies as opposed to the case of the previously reported BiTeI [50]. We employed the $\mathbf{k} \cdot \mathbf{p}$ approximation near the Γ point to further understand the conduction band states. The high-symmetry phase was explored in a previous study [51]; therefore we focus only on the ferroelectric phase. The details of our DFT-based results (both PE and FE cases) are reported in the Supplemental Material [32] along with a discussion about the symmetry-induced protection of the spin state (see also

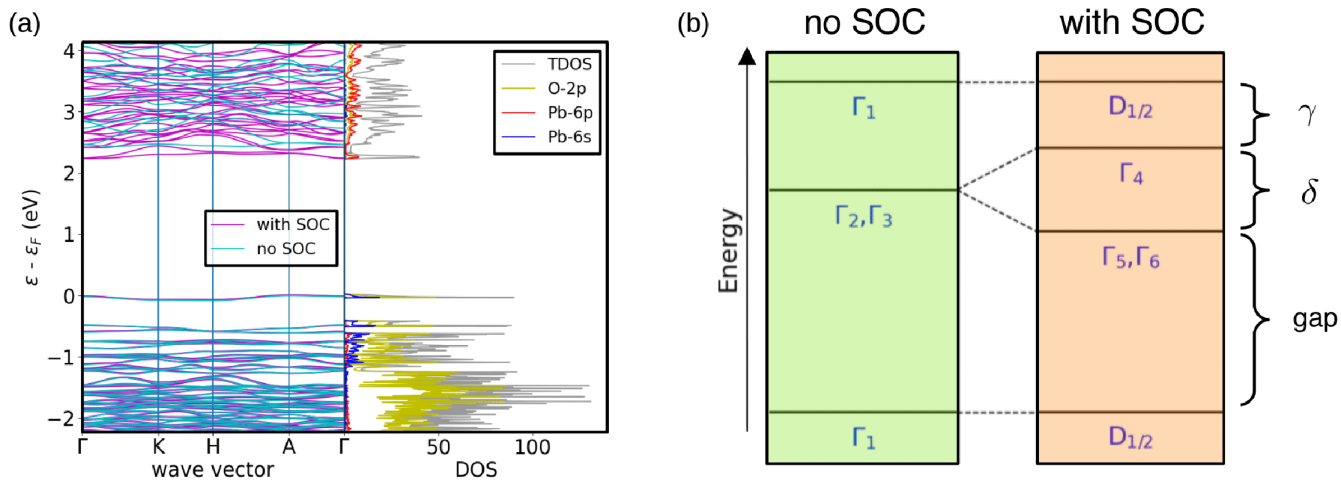

FIG. 2. (a) Band structure (left) and orbital-projected density of states (right) of the ferroelectric $P3$ phase. The SOC splitting is clearly evident in the bottom conduction bands. (b) A schematic of the spin-orbit-coupling-induced splitting (single to double irreducible representation) of the CBM and VBM levels for the FE phase. The IR labels of the C_{3h} and C_3 point groups are the same as in the Bilbao Crystallographic Server, while D is the SO(3) × {1, −1} spin representation reduced to threefold rotations and the z-mirror inversion. TDOS, total density of states.

Refs. [52–54] and Refs. [16,55]). The spin-orbit part of the $P3$ phase ($\bar{\Gamma}_5 \oplus \bar{\Gamma}_6$) can be described by

$$H_{P3}^{\mathrm{SOC}}(\mathbf{k}) = \lambda_R(k_y\sigma_x - k_x\sigma_y) + \sum_{i=x,y,z} \lambda_{W_i} k_i \sigma_i, \qquad (1)$$

where λ_R (−0.10 eV Å) is the Rashba interaction strength and where $\lambda_{W_x} = \lambda_{W_y} \equiv \lambda_w$ (0.11 eV Å) and λ_{W_z} (0.01 eV Å) represent a Weyl-type band spin splitting, where σ labels the spin. We define $\alpha = \sqrt{\lambda_R^2 + \lambda_w^2}$ (0.15 eV Å) to easily quantify the SOC strength. The values of the SOC parameters are comparable to those of Bi_2WO_6, $BiAlO_3$, GeTe, or BiTeI [27], and they are one order of magnitude larger than the values reported in a recent work on $LaAlO_3/LaFeO_3/SrTiO_3$ [56]. Furthermore, exploiting the SOC in this material can be achieved without the need to engineer the unit cell, as it may occur with certain tungsten oxide compounds such as WO_3, which requires confinement in the direction perpendicular to the polarization [27]. The symmetries of the $P3$ space group allow for an electric-field-switchable [17] momentum-dependent [32,57] spin texture, and because polar domains of PGO are optically active, this suggests the possibility of controlling the handedness of the spin texture with chiral light. It is likely that an electric bias could also be used to tune λ_R, whereas at the same time a magnetic Zeeman interaction may be employed to displace but not remove the crossing between the spin bands. In particular, we realize [32] that this crossing is protected [58,59] by a $\mathbb{Z}_2$ topological number because of the presence of a Weyl point at Γ, which means that the degeneracy of the spin cannot be removed by a magnetic field.

We are left with the need for a microscopic explanation of the large SOC effects. We have seen that SOC mainly affects the conduction bands owing to its predominant Pb-6p character. To gain further insight, we show in Fig. 3 the band-projected charge density corresponding to isolated bands—a top VB and a bottom CB—in the $P3$ phase. We find that the top valence electrons are mainly localized at the Pb-1c site and the O-6l sites (sp hybridization), the latter bonding with the Ge_2O_7 units and Pb-1c and Pb-2h atoms. This localization near the Ge_2O_7 dimers is due to the Pb-6s states associated with the steep DOS peak at the Fermi level, which corresponds to the 1c WP. On the other hand, the bottom-CB charge (where SOC splitting is the most apparent with Pb-6p character) is found to be mostly localized in the vacuum channel, and it comes from the Pb-6l WPs that are around the cavity. It is striking to see in Fig. 3 that this CB of the Pb-6l sites forms a unique and complex cavity state that is quite different from the atomic 6p orbital shapes. It is also interesting to notice that this cavity state exhibits large SOC features due to its cavity localization and unquenched **L**. We further highlight the presence of this phenomenon—independent from any mirror operation—in the $P\bar{6}$ phase as well [32].

To scrutinize the origin of the large SOC observed in PGO, we performed computer experiments by switching the SOC on and off on selected orbitals and at selected atomic sites. For each case, we recalculated the ferroelectric double-well depth ΔE and several SOC-related parameters of interest (including the aforementioned δ, γ, and α), as well as the band gap. The results are reported in Tables SIII and SIV of the Supplemental Material [32]. These results also indicate that the relatively small hybridization of the Pb-6p states with Pb-6s and O-2p states is responsible for the SOC renormalization of the energy landscape, as the empty states (CB) do not contribute to the energy. They also explain the aforementioned negative correlation of ΔE with the gap size. Now, for the six different Pb WPs of the $P\bar{6}$ phase, we observe that deactivating the SOC at the 3k sites significantly affects the PE-FE energy barrier (∼17% decrease) compared with the 6l, 1c, 1e, 2i, and 2h WPs ($\lesssim$7% variation). A reason for this—along with the aforementioned Pb-O interaction—can be attributed to the fact that the site symmetry group associated with the 3k WPs is m, which is broken by the phase transition, while the site symmetries induced by the other Pb positions are preserved. On the other hand, the spin-splitting and split-off CB parameters do not necessarily follow this trend because deactivating the SOC at the 1c, 1e, and 2i sites can produce a 2 or 3 times

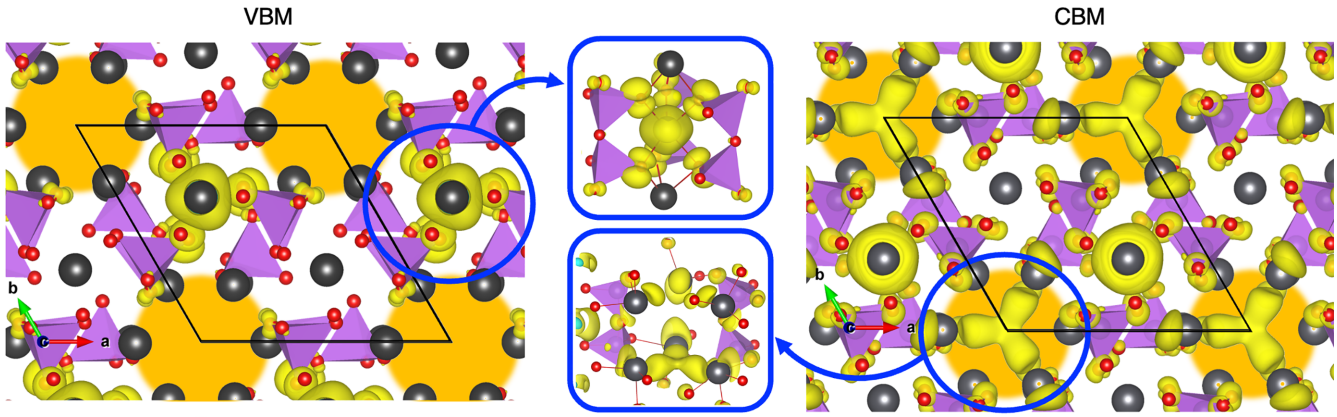

FIG. 3. Ferroelectric partial charge density associated with the VBM (isosurface = 0.001) and CBM (isosurface = 0.0005) energy window states (projected density of states peaks in Fig. 2). Lead and oxygen atoms are shown in black and red, respectively. GeO_4 tetrahedra are shown in purple, and empty channels are evidenced in gold.

increase in the α parameter (for example, $\Delta E = 87$ meV and $\alpha = 0.29$ eV Å in the $2i$-off case). Overall, the substitution (alloying) at the selected WP could either affect the ferroelectric domain barrier and/or the CB parameters (spin and band splitting) in a broad fashion, provided that further lowering of the symmetry (if present) and chemical changes have a small impact on the electronic states.

Finally, we discuss the robustness of the phase transition under doping. Exploiting the Rashba phenomenology requires, on the one hand, the breaking of the inversion symmetry and, on the other hand, the presence of free carriers, which tend to screen long-range forces responsible for polar instability [27,60] and thus reduce the magnitude of the spin-splitting parameters. We have thus introduced some charge in the unit cell and performed the relaxation of the atomic positions, without relaxing the cell parameters at the same time (as the internal pressure is not well defined for charged systems in periodic boundary conditions [61]). Then we have calculated ΔE as a function of p- and n-type carrier doping concentrations (see Fig. 4). In contrast to regular ferroelectrics [60], ΔE is surprisingly enhanced by n-type doping of the CBM states. The calculation [62–64] of the phonons reveals [32] that the polar instability has a short-range origin. Hence the screening of the Coulomb interaction by charges does not affect the instability, as in $BaTiO_3$ [62]. However, depopulating the VBM (p-type doping) can stabilize the paraelectric phase above a concentration of ∼0.66 holes/f.u., which highlights the importance of the VBM Pb-6s orbitals for the stabilization of the $P3$ phase. Finally, we find that the ferroelectric phase is further stabilized in the n-type doping (plus one electron) scenario when the spin polarization is included [32]. The extra electron localizes inside the Pb-6p cavity states (Fig. 9 of Ref. [32]) and possesses a magnetic moment which could be analyzed in photoexcitation experiments. Moreover, the localization of these states could provide the necessary coherence for qubit manipulation, also to be probed in future experimental works.

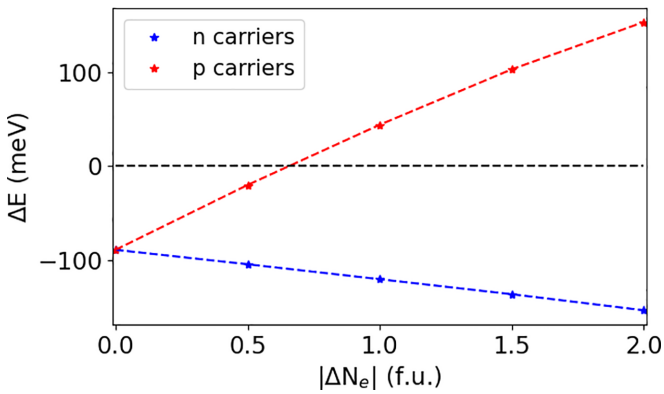

FIG. 4. $\Delta E = E(\mathrm{FE}) - E(\mathrm{PE})$ as a function of extra n- and p-type charge. While an increasing negative carrier concentration lowers the $P3$ phase energy even further with respect to the paraelectric case, the $P\bar{6}$ phase can be stabilized instead with a hole concentration above ∼0.655 f.u.

In conclusion, we have shown that the ferroelectric material $Pb_5Ge_3O_{11}$ can be used as a single platform for controlling diverse spin-orbital properties. We find a large SOC-induced renormalization of the ferroelectric double well, which originates from the O-2p–Pb-6p overlap along with the breaking of the mirror site symmetry at the Pb-3k positions. Symmetry analysis shows that the FE structure leads to mixed Rashba-Weyl spin splitting with $\mathbb{Z}_2$ topological protection. We argue that the asymmetric localization of the 6p states inside the cavity channel, along with the large atomic number Z of Pb and first-order nature of the SOC energy correction, can produce large spin-orbital effects. The deactivation of the SOC at selected WPs also reveals a wide degree of control over the domain barrier and conduction band parameters. This makes PGO an interesting platform for tuning and designing different SOC effects in a way that complements the approach based on the Hubbard-U induced localization and **L** unquenching of half-filled valence bands depicted in Ref. [65]. The localization of the bottom CB levels stems from the presence of natural empty channels and, along with the short-range character of the driving forces of the phase transition, supports ferroelectricity under n-type doping conditions. Hence the resulting design rule to obtain large SOC effects in crystals containing Pb^{2+} or Bi^{3+} cations would be to have them placed

at the edge of a cavity to form unquenched 6p cavity states. This condition could potentially be explored in other materials with a similar crystal structure where natural empty channels are present, e.g., in $Pb_5(SiO_4)(VO_4)_2$ [66]. Exploiting the properties of the cavity-confined Pb-6p conduction orbitals would require photoexcitation techniques and/or doping, although alloying may be used as an exploratory method as well. Being relatively confined, these wave functions may host novel and unexplored optoelectronic and quantum properties. If we assume a possible dependence on geometrical features, it would be interesting to further explore how the aforementioned states are affected by the size and the shape of the cavity enclosing them.

The authors acknowledge E. McCabe, Z. Romestan, and S. Bandyopadhyay for fruitful discussions. Computational resources were provided by the Consortium des Équipements de Calcul Intensif (CÉCI), funded by the Fonds de la Recherche Scientifique (F.R.S.-FNRS) under Grant No. 2.5020.11. M.F. and E.B. acknowledge FNRS for support and the PDR project CHRYSALID, No. 40003544. Work at West Virginia University was supported by the U.S. Department of Energy (DOE), Office of Science, Basic Energy Sciences (BES), under Award No. DE-SC0021375. We also acknowledge the computational resources awarded by XSEDE, a project supported by National Science Foundation Grant No. ACI-1053575. The authors also acknowledge the support from the Texas Advanced Computing Center (with the Stampede2 and Bridges supercomputers). We also acknowledge the supercomputing system (Thorny Flat) at WVU, which is funded in part by West Virginia University and the National Science Foundation (NSF) under Grant No. 1726534.

[1] J. Stöhr and H. C. Siegmann, *Magnetism: From Fundamentals to Nanoscale Dynamics* (Springer, Berlin, 2006).
[2] A. Manchon, J. Železný, I. M. Miron, T. Jungwirth, J. Sinova, A. Thiaville, K. Garello, and P. Gambardella, Rev. Mod. Phys. **91**, 035004 (2019).
[3] P. Gambardella and I. M. Miron, Philos. Trans. R. Soc. A **369**, 3175 (2011).
[4] Y. Tokura and N. Kanazawa, Chem. Rev. **121**, 2857 (2021).
[5] K. Everschor-Sitte, J. Masell, R. M. Reeve, and M. Kläui, J. Appl. Phys. **124**, 240901 (2018).
[6] A. Fert, N. Reyren, and V. Cros, Nat. Rev. Mater. **2**, 17031 (2017).
[7] M. Z. Hasan and C. L. Kane, Rev. Mod. Phys. **82**, 3045 (2010).
[8] X.-L. Qi and S.-C. Zhang, Rev. Mod. Phys. **83**, 1057 (2011).
[9] S. Murakami, N. Nagaosa, and S.-C. Zhang, Science **301**, 1348 (2003).
[10] J. Sinova, D. Culcer, Q. Niu, N. A. Sinitsyn, T. Jungwirth, and A. H. MacDonald, Phys. Rev. Lett. **92**, 126603 (2004).
[11] Y. K. Kato, R. C. Myers, A. C. Gossard, and D. D. Awschalom, Science **306**, 1910 (2004).
[12] B. A. Bernevig and S.-C. Zhang, Phys. Rev. Lett. **96**, 106802 (2006).
[13] J. D. Koralek, C. P. Weber, J. Orenstein, B. A. Bernevig, S.-C. Zhang, S. Mack, and D. D. Awschalom, Nature (London) **458**, 610 (2009).
[14] M. P. Walser, C. Reichl, W. Wegscheider, and G. Salis, Nat. Phys. **8**, 757 (2012).
[15] A. Sasaki, S. Nonaka, Y. Kunihashi, M. Kohda, T. Bauernfeind, T. Dollinger, K. Richter, and J. Nitta, Nat. Nanotechnol. **9**, 703 (2014).
[16] L. L. Tao and E. Y. Tsymbal, Nat. Commun. **9**, 2763 (2018).
[17] L. L. Tao and E. Y. Tsymbal, J. Phys. D: Appl. Phys. **54**, 113001 (2021).
[18] G. Bihlmayer, O. Rader, and R. Winkler, New J. Phys. **17**, 050202 (2015).
[19] Y. A. Bychkov and E. I. Rashba, J. Phys. C: Solid State Phys. **17**, 6039 (1984).
[20] D. Di Sante, P. Barone, R. Bertacco, and S. Picozzi, Adv. Mater. **25**, 509 (2013).
[21] L. L. Tao, T. R. Paudel, A. A. Kovalev, and E. Y. Tsymbal, Phys. Rev. B **95**, 245141 (2017).
[22] G. Dresselhaus, Phys. Rev. **100**, 580 (1955).
[23] R. Moriya, K. Sawano, Y. Hoshi, S. Masubuchi, Y. Shiraki, A. Wild, C. Neumann, G. Abstreiter, D. Bougeard, T. Koga, and T. Machida, Phys. Rev. Lett. **113**, 086601 (2014).
[24] H. Nakamura, T. Koga, and T. Kimura, Phys. Rev. Lett. **108**, 206601 (2012).
[25] M. Gmitra and J. Fabian, Phys. Rev. B **94**, 165202 (2016).
[26] F. Trier, P. Noël, J.-V. Kim, J.-P. Attané, L. Vila, and M. Bibes, Nat. Rev. Mater. **7**, 258 (2022).
[27] H. Djani, A. C. Garcia-Castro, W.-Y. Tong, P. Barone, E. Bousquet, S. Picozzi, and P. Ghosez, npj Quantum Mater. **4**, 51 (2019).
[28] J. Hlinka, J. Privratska, P. Ondrejkovic, and V. Janovec, Phys. Rev. Lett. **116**, 177602 (2016).
[29] T. Hayashida, Y. Uemura, K. Kimura, S. Matsuoka, D. Morikawa, S. Hirose, K. Tsuda, T. Hasegawa, and T. Kimura, Nat. Commun. **11**, 4582 (2020).
[30] H. Iwasaki, K. Sugii, T. Yamada, and N. Niizeki, Appl. Phys. Lett. **18**, 444 (1971).
[31] H. Iwasaki, S. Miyazawa, H. Koizumi, K. Sugii, and N. Niizeki, J. Appl. Phys. **43**, 4907 (1972).
[32] See Supplemental Material at http://link.aps.org/supplemental/10.1103/PhysRevB.108.L201112 for more details concerning the computational details, structural information, PE frequency calculations, electronic properties, symmetry analysis, $\mathbf{k}\cdot\mathbf{p}$ model, $P3$ spin textures, $\mathbb{Z}_2$ topological number, and FE-PE barrier.
[33] X. Gonze, F. Jollet, F. Abreu Araujo, D. Adams, B. Amadon, T. Applencourt, C. Audouze, J.-M. Beuken, J. Bieder, A. Bokhanchuk, E. Bousquet, F. Bruneval, D. Caliste, M. Côte, F. Dahm, F. Da Pieve, M. Delaveau, M. Di Gennaro, B. Dorado, C. Espejo *et al.*, Comput. Phys. Commun. **205**, 106 (2016).
[34] X. Gonze, B. Amadon, G. Antonius, F. Arnardi, L. Baguet, J.-M. Beuken, J. Bieder, F. Bottin, J. Bouchet, E. Bousquet, N. Brouwer, F. Bruneval, G. Brunin, T. Cavignac, J.-B. Charraud, W. Chen, M. Côté, S. Cottenier, J. Denier, G. Geneste *et al.*, Comput. Phys. Commun. **248**, 107042 (2020).

[35] M. J. van Setten, M. Giantomassi, E. Bousquet, M. J. Verstraete, D. R. Hamann, X. Gonze, and G.-M. Rignanese, Comput. Phys. Commun. **226**, 39 (2018).
[36] J. P. Perdew, K. Burke, and M. Ernzerhof, Phys. Rev. Lett. **77**, 3865 (1996).
[37] J. P. Perdew, A. Ruzsinszky, G. I. Csonka, O. A. Vydrov, G. E. Scuseria, L. A. Constantin, X. Zhou, and K. Burke, Phys. Rev. Lett. **100**, 136406 (2008).
[38] G. Kresse and D. Joubert, Phys. Rev. B **59**, 1758 (1999).
[39] K. Momma and F. Izumi, J. Appl. Crystallogr. **44**, 1272 (2011).
[40] R. Viennois, I. Kityk, A. Majchrowski, J. Zmija, Z. Mierczyk, and P. Papet, Mater. Chem. Phys. **213**, 461 (2018).
[41] C. Konak, V. Kopsky, and F. Smutny, J. Phys. C: Solid State Phys. **11**, 2493 (1978).
[42] O. G. Vlokh, Ferroelectrics **75**, 119 (1987).
[43] Y. Iwata, J. Phys. Soc. Jpn. **43**, 961 (1977).
[44] R. Newnham, R. Wolfe, and C. Darlington, J. Solid State Chem. **6**, 378 (1973).
[45] R. Arras, J. Gosteau, H. J. Zhao, C. Paillard, Y. Yang, and L. Bellaiche, Phys. Rev. B **100**, 174415 (2019).
[46] S. C. Sabharwal, S. N. Jha, and Sangeeta, Bull. Mater. Sci. **33**, 395 (2010).
[47] X. Wu, J. Xu, J. Xiao, A. Wu, and W. Jin, J. Cryst. Growth **263**, 208 (2004).
[48] T. Rangel, D. Kecik, P. E. Trevisanutto, G.-M. Rignanese, H. Van Swygenhoven, and V. Olevano, Phys. Rev. B **86**, 125125 (2012).
[49] M. Hussain, M. Rashid, F. Saeed, and A. S. Bhatti, J. Mater. Sci. **56**, 528 (2021).
[50] M. S. Bahramy, R. Arita, and N. Nagaosa, Phys. Rev. B **84**, 041202(R) (2011).
[51] H. J. Zhao, H. Nakamura, R. Arras, C. Paillard, P. Chen, J. Gosteau, X. Li, Y. Yang, and L. Bellaiche, Phys. Rev. Lett. **125**, 216405 (2020).
[52] R. J. Elliott, Phys. Rev. **96**, 266 (1954).
[53] Y. Yafet, Solid State Phys. **14**, 1 (1963).
[54] M. I. D'Yakonov and V. I. Perel', Sov. J. Exp. Theor. Phys. **33**, 1053 (1971).
[55] B. A. Bernevig, J. Orenstein, and S.-C. Zhang, Phys. Rev. Lett. **97**, 236601 (2006).
[56] G. J. Omar, W. L. Kong, H. Jani, M. S. Li, J. Zhou, Z. S. Lim, S. Prakash, S. W. Zeng, S. Hooda, T. Venkatesan, Y. P. Feng, S. J. Pennycook, L. Shen, and A. Ariando, Phys. Rev. Lett. **129**, 187203 (2022).
[57] U. Herath, P. Tavadze, X. He, E. Bousquet, S. Singh, F. Muñoz, and A. H. Romero, Comput. Phys. Commun. **251**, 107080 (2020).
[58] D. Gresch, G. Autès, O. V. Yazyev, M. Troyer, D. Vanderbilt, B. A. Bernevig, and A. A. Soluyanov, Phys. Rev. B **95**, 075146 (2017).
[59] A. A. Soluyanov and D. Vanderbilt, Phys. Rev. B **83**, 235401 (2011).
[60] Y. Wang, X. Liu, J. D. Burton, S. S. Jaswal, and E. Y. Tsymbal, Phys. Rev. Lett. **109**, 247601 (2012).
[61] F. Bruneval, C. Varvenne, J.-P. Crocombette, and E. Clouet, Phys. Rev. B **91**, 024107 (2015).
[62] P. Ghosez, X. Gonze, and J.-P. Michenaud, Europhys. Lett. **33**, 713 (1996).
[63] X. Gonze and C. Lee, Phys. Rev. B **55**, 10355 (1997).
[64] E. Bousquet and P. Ghosez, Phys. Rev. B **74**, 180101(R) (2006).
[65] J. Li, Q. Yao, L. Wu, Z. Hu, B. Gao, X. Wan, and Q. Liu, Nat. Commun. **13**, 919 (2022).
[66] S. Krivovichev, T. Armbruster, and W. Depmeier, Mater. Res. Bull. **39**, 1717 (2004).

Correction: An error appeared in the α value in the penultimate sentence of the paragraph that begins "To scrutinize" and has been fixed.